Supplemental Methods

Primary cells from leukemia patients and healthy donors

Fresh leukapheresis or peripheral blood samples from patients with newly diagnosed CML-CP, from CML-AP, and from healthy donors were obtained from the Paul O'Gorman Leukemia Research Centre, University of Glasgow, Glasgow, UK, and from the Stem Cell and Leukemia Core Facility of the University of Pennsylvania, Philadelphia, PA, USA (**Table S1**). Additional samples of normal hematopietic cells were purchased from Cambrex Bio Science (Walkersville, MD, USA). Lin-CD34+ cells were obtained from mononuclears by magnetic sorting using the EasySep negative selection human progenitor cell enrichment cocktail followed by human CD34 positive selection cocktail (StemCell Technologies). Leukapheresis samples were enriched for $CD34^+$ cells using CliniMACS (Miltenyi Biotec Ltd). To assay expansion, colony forming cells (CFCs) and microarray-probed gene expression, $CD34^+$ cells were cultured overnight in serum free medium (SFM) consisting of Iscove's Modified Dulbecco's Medium (IMDM, Sigma-Aldrich) containing a serum substitute (bovine serum albumin [BSA], insulin, transferrin [BIT]; StemCell Technologies), 0.1μM 2-mercaptoethanol (Sigma-Aldrich), ± a high concentration five growth factor (5GF) cocktail comprising 100ng/mL Flt3-ligand (Flt3L), 100ng/mL stem cell factor (SCF), and 20ng/mL each of interleukin (IL)-3, IL-6 (all from StemCell Technologies) and granulocyte-colony stimulating factor (G-CSF; Chugai Pharma Europe). $CD34^+$ CML and normal cells were simultaneously stained with lineage (lin) cocktail-FITC, CD90-PE, CD34PerCP, CD38PE-Cy7, CD123-APC and CD45RA-Pacific Blue (all BD Biosciences) at room temperature (RT) for 20 minutes. Unbound antibodies were washed off with PBS/2% fetal calf serum (FCS) and the cells were FACS-sorted to isolate the different subpopulations (hematopoietic stem cell [HSC]– $lin^-CD34^+CD38^-CD90^+$; multipotent progenitor [MPP] - $lin^-CD34^+CD38^-CD90^-$; common myeloid progenitor [CMP] – $lin^-CD34^+CD38^+CD123^+CD45RA^-$; granulocyte monocyte progenitor [GMP] – $lin^-CD34^+CD38^+CD123^+CD45RA^{lo}$; and megakaryocyte erythroid progenitor [MEP] – $lin^-CD34^+CD38^+CD123^-CD45RA^-$) using FACSAria (BD Biosciences). After enumeration, colony forming cell (CFC) and expansion assays were performed. In brief, 2000 cells from each subpopulation were set up in duplicate in 1mL of Methocult (StemCell Technologies) or cultured in SFM supplemented with a low growth factor cocktail comprising 5ng/mL Flt3L, 5ng/mL SCF, and 1ng/mL of each IL-3, IL-6 and G-CSF. Acute myeloid leukemia (AML), B- and T- cell acute lymphoblastic leukemia (B-ALL and T-ALL, respectively) were obtained from patients after informed consent (**Table S2, S3**) and injected i.v. into NSG mice. Bone marrow and spleen xenografts containing >80% and >90% of AML and ALL cells, respectively, were tested for BRCA1 and BRCA2 mRNA expression levels. Acute promyelocytic leukemia (APL) samples were purchased from the Stem Cell and Leukemia Core Facility of the University of Pennsylvania, Philadelphia, PA, USA (**Table S4**). The studies were approved by the appropriate Institutional Review Boards.

Rad52-/- and *Rad52+/+* cells

Rad52$^{+/+}$ and *Rad52*$^{-/-}$ transgenic mice [1] were generously provided by Maria Jasin (Sloan Kettering Cancer Center, New York, NY, USA). Bone marrow mononuclear cells were obtained by centrifugation on Lympholyte-M (Cedarlane). $Lin^-c\text{-}Kit^+Sca\text{-}1^+$ LSCs were identified by immunofluorescent staining using PerCP-Cy5.5-conjugated anti-lineage cocktail (CD3e, CD11b, CD45R/B220, Ly-76, Ly-6G, and Ly6C), PE-conjugated anti-c-Kit, and PE-Cy7-conjugated anti-Sca-1 (BD Pharmingen). PE-conjugated anti-CD34 and APC-conjugated anti-Flt3 antibodies (BD Pharmingen) were used to identify long-term ($Lin^-c\text{-}Kit^+Sca\text{-}1^+CD34^-Flt3^-$) and short-term ($Lin^-c\text{-}Kit^+Sca\text{-}1^+CD34^+Flt3^-$) LSCs (LT-LSCs and ST-LSCs, respectively). Murine hematopoietic cells were cultured in IMDM with 10% FBS supplemented with pre-tested threshold concentrations of IL-3 and SCF necessary to support proliferation of normal cells [2]; 200 μM of vitamin E (VE) or 50 μM of N-acetyl-L-cysteine (NAC) was added when indicated [3]. Cell cycle progression was examined using propidium iodide (Sigma) as described before [4]. Clonogenic activity was measured in Methocult™ (StemCell Technologies) in the presence of IL-3 and SCF.

Leukemogenesis *in vivo*

Rad52+/+ or *Rad52*-/- murine bone marrow mononuclear cells were infected with pMIG-BCR-ABL1-IRES-GFP retroviral particles as described before [2]. GFP+ cells were injected via tail vein in to sub-lethally irradiated NOD/SCID mice. Animals were sacrificed when signs of morbidity were apparent and leukemia development

was confirmed on necropsy. These studies were approved by the Institutional Animal Care and Use Committee.

Cell lines

Murine hematopoietic 32Dcl3 cell line (32D) and BCR-ABL1-positive 32Dcl3 cells (B/A-32D), and PML-RAR –positive NB4 cell line were maintained as previously described [2,5]. Human megakaryocytic UT7 cells and their BCR-ABL1 –positive counterparts were maintained in IMDM supplemented with 10% FBS and 5 ng/ml human granulocyte-macrophage colony-stimulating factor (GM-CSF; PeproTech, Rocky Hill, NJ, USA) [6]. Capan-1, a pancreatic carcinoma cell line with truncated *BRCA2* (*BRCA2Δ/-*) as well as Capan-1 cells in which BRCA2 expression has been restored (*BRCA2+*) were obtained from Dr. Simon Powell [7]. Human ovarian carcinoma cell line UWB1.289 carrying a germ-line *BRCA1* mutation within exon 11 (2594delC) and a deletion of the wild-type allele (*BRCA1-null*), and UWB1.289 cells with restored BRCA1 expression (*BRCA1+*) were described before and purchased from ATCC [8]. Breast cancer cell line, HCC1937, (5382insC germ-line mutation generating the truncated protein and no wild-type allele, *BRCA1-null*) and cells with restored BRCA1 expression (*BRCA1+*) were obtained from Dr Ralph Scully [9].

RNA preparation and microarray analysis

RNA was prepared from sorted subpopulations of cells using the RNEasy mini-kit or micro-kit (Qiagen) depending on cell number. RNA samples were analyzed on the Affymetrix GeneChip Human Gene 1.0 ST arrays using standard Affymetrix protocols. The raw data CEL files were normalized using gcRMA n Partek Genomic Suite http://www.partek.com/partekgs software or using a function for "quantile" normalization in the "limma" package in R program. One way ANOVA was performed on the imported, normalized and summarized microarray data to find differently expressed genes between all cell subpopulations and disease states. Lists of differentially expressed genes were created using an FDR limit of 0.05 to control for multiple comparisons but no limit on degree of fold change. These lists were uploaded directly into Ingenuity Pathway Analysis (IPA) software (Ingenuity® Systems). To determine which functional groupings of genes were differentially expressed we performed gene ontology ANOVA (GO ANOVA). Partek GS utilizes the gene ontology database to map genes to standardized functional groupings. The ANOVA model was configured to contrast the different sub populations and disease states in order to determine the significance and average fold change of each GO category across all the comparator groups. These results were visualized using dot plots where the average expression of all genes in that functional group is represented as a single dot. The average expression is plotted on a log2 scale on the y axis – and each subpopulation in each disease state on the x axis. The CML microarray protocol was published before [10].

Validation of the microarray analysis

We validated the results from the microarray using the Fluidigm microfluidic dynamic array qRT-PCR platform. Briefly, 200 ng of RNA from each subpopulation analysed in the microarray experiments described previously was reverse transcribed using the applied biosystems high capacity RT kit under standard conditions to produce 20 μL of cDNA solution. A 5 μL aliquot of each sample was amplified over 14 cycles using the applied biosystems pre-amplification kit and applied biosytems taqman probe sets. Following pre-amplification the resultant amplified products were loaded in triplicate onto 2 primed 48x48 fluidigm microfluidic dynamic arrays. The desired taqman probe sets were loaded onto the chip. The assays and samples are automatically combined on chip prior to thermal cycling and fluorescence detection. This allows the comparison of 48 assays across 15 samples in triplicate and 1 in duplicate. We included a common sample across chips to ensure that inter chip variation was minimal. Amplification curves were produced for each reaction, and expression levels calculated from the mean cycle threshold (C_t) of each triplicate reaction. We utilized HRPT1 and GAPDH as endogenous control genes, calculating the ΔC_t as the $C_{t(target)}$ minus the geometric mean of $C_{t(HRPT1)}$ and $C_{t(GAPDH)}$. We expressed the fold change as 2 to the power of the negative difference between the ΔC_t of the target sample and the mean of all the non CML samples i.e. ($2^{-(\Delta Ct[\text{CML sample}]) - (\text{mean } \Delta Ct\ [\text{Non CML samples}])}$).

Quantitative RT-PCR (qRT-PCR)

Total RNA from human leukemia cells was extracted using RNeasy isolation kit from QIAGEN according to the manufacturer's instructions. cDNA was generated using a poly(dT) oligonucleotide and the SuperScript III Reverse transcription according to the manufacturer's protocol (Invitrogen). The levels of gene expression

were measured using the SYBRGreenER mix (Invitrogen) with the following sets of primers: BRCA1: sense-GGAGGTCAGGAGTTCGAAACC, antisense-ACCGGCTAATTTCTGTATTTTTAGTAGAG; BRCA2: sense-ACCTGTTAGTCCCATTTGTACATTTG, antisense-CACAACTCCTTGGTGGCTGAA; and COX6B: sense-AACTACAAGACCGCCCCTTT, antisense-GCAGCCAGTTCAGATCTTCC. The reactions were performed in and the ABI7900HT real-time PCR system (Applied Biosystems) and analyzed with SigmaPlot version 12.0 software program.

RT-PCR

Total RNA from 10^6 BMCs was extracted using the QIAamp RNA Blood Mini Kit (Qiagen). cDNA was used to amplify an 863bp fragment of the human ABL1 kinase domain (forward 5'-CGCAACAAGCCCACTGTC-3' and reverse 5'-TCCACTTCGTCTGAGATACTGGATT-3') as described before [3]. Two identical rounds of PCR were conducted in which ¼ of the original reaction mixture was used in the second PCR reaction. A 487bp fragment of glyceraldehyde-3-phosphate (GAPDH) cDNA was amplified (forward 5'-ACCACAGTCCATGCCATCAC-3' and reverse 5'-TCCACCACCCTGTTGCTGTA-3') as a loading control. The products were analyzed in agarose gel electrophoresis. This PCR method detected 10^2 BCR-ABL1 -positive cells in 10^6 total cells.

Immunoprecipitation and Western analyses

Total and nuclear cell extracts were prepared as described before [11,12]. Anti-Flag immunoprecipitates were obtained as described before [11]. Lysates and immunoprecipitates were analyzed by SDS-PAGE followed by Western blotting using antibodies detecting ABL1 (EMD Chemicals, Inc), phosphotyrosine (Milipore), BRCA1 (R&D Systems), RAD51C and lamin B (both from Abcam).

BRCA1 immunofluorescence

Differences in BRCA1 protein expression levels in AML, B-ALL and T-ALL xenografts were confirmed by immunofluorescence as described before [13]. Briefly, cells were cytospun and stained with anti-BRCA1 antibody (Millipore) and Ki-67 antibody (Abcam) followed by secondary antibodies conjugated with AlexaFluor 488 or 594. DNA was counterstained with 4',6'diamidino-2-phenylindole (DAPI, Invitrogen). Cells were visualized in a Nikon Eclipse E300 fluorescent microscope equipped with digital camera. Images from 25-50 cells/group were processed using SlideBook version 3.0 (Intelligent Imaging Innovation) and Adobe Photoshop version 6.0 software (Adobe Systems).

Nuclear foci

Cells were irradiated, or not, with 4Gy from RS-2000 Biological Research Irradiator (RadSource Technologies, Inc.) and 3 hours later cytospins were prepared using polylysine coated slides (Thermo Scientific) and fixed as described before [14]. Nuclear foci were detected by staining with primary antibodies against RAD51, RAD52 (Cell Signalling), BRCA1 (Calbiochem) and γ-H2AX (Millipore) followed by the secondary antibodies conjugated to Alexa Fluor 594 or 488 (Molecular Probes). DNA was counterstained with DAPI. Staining and images from 25-50 cells/group were processed using SlideBook 3.0 and Adobe Photoshop 6.0 software as described before [14].

ssDNA binding

The assay was performed as described by Grimme and colleagues with modifications [15]. Briefly, 30-mer ssDNA oligonucleotide was HPLC purified and 5' end-labelled with IRDye800 (5IRD800-AAG TGA ACA TAA AGT AAA TAA GTA TAA CGA) (Integrated DNA Technologies). 20 nM of IRDye800-labelled DNA substrate was incubated with GST-hRAD52 in specific binding buffer [10mM Tris (pH 7.5), 50 mM KCl, 2.5 mM DTT/0.25% Tween 20, 0.1 mg/ml BSA] or with GST-hRAD51 in specific binding buffer [same as above + 1mM ATP and 2mM $MgCl_2$]. When indicated, 0.25 mM of F79 or F79A aptamer was added. The reaction mixtures (20 μl) were incubated at 37°C for 15 minutes to allow for the formation of the DNA-protein complex. Glycerol was added to the samples at a final concentration of 2% before analysis on an 8% native polyacrylamide gel. The reaction products were imaged using an Odyssey Infrared Imager (LI-COR Biosciences). The presence of RAD52 and RAD51 proteins in the shifted products was confirmed by Western blot with anti-RAD52 and anti-RAD51 antibody (Santa Cruz Biotechnology).

HRR Assay

32Dcl3 parental cells and their BCR-ABL1-transformed counterparts carrying a single copy of DR-GFP recombination cassette were described before [4]. Cells were infected with retroviral constructs pMIG-Flag-RAD51(WT)-IRES-DsRed or pMIG-Flag-RAD51(F259V)-IRES-DsRed, and expression of Flag-tagged exogenous RAD51 proteins were confirmed by anti-Flag immunofluorescence. DsRed+ cells were then electroporated with 100μg of pCβA-Sce expression plasmid encoding I-*Sce*I endonuclease (pMIG-IRES-GFP plasmid was used to detect transfection efficiency on separate sample). HRR of the I-*Sce*I -induced DSB in DR-GFP cassette restores functional GFP expression, which is readily detected 48h after transfection with I-*Sce*I. The percentage of GFP+DsRed+ double-positive cells in DsRed+ population was detected by flow cytometry to assess HRR repair activity.

NHEJ reaction

The assay was performed as described before [4]. Briefly, nuclear lysate from BCR-ABL1-positive 3Dcl3 cells were mixed with *XhoI+XbaI* –linearized pBluescript KS (to create non-compatible DSB ends) and 0.25 mM F79 when indicated. The products were visualized by agarose gel electrophoresis containing ethidium bromide and scanned with Adobe Photoshop.

DNA constructs

pMIG-IRES-GFP or pMIG-BCR-ABL1-IRES-GFP were obtained from Dr. Warren Pear (University of Pennsylvania, Philadelphia, PA, USA). pGEX-4T2 containing GST-hRAD51 was described before [11]. GST-hRAD52 was obtained from Alan Tompkinson (University of New Mexico Cancer Center, Albuquerque, NM, USA). RAD51-Flag wild-type (WT) was cloned into pMIG-IRES-GFP and pMIG-IRES-DsRed. The F259V mutation was introduced to the RAD51-Flag cDNA by the QuikChange II XL site-directed mutagenesis kit (Stratagene/Agilent Technologies). The pLSXP-GFP/RAD52 retroviral construct was generously provided by Zhiyuan Shen (The Cancer Institute of New Jersey, New Brunswick, NJ, USA). The GFP sequence in GFP/RAD52 fusion gene was mutated to YFP (T203Y) by the QuikChange II Site Directed Mutagenesis kit. The point mutations within the RAD52 sequence were made separately in pLXSP-YFP/RAD52 and pEGFPN1/RAD52 constructs (F79A, K102A, and Y104F) using the QuikChange kit. The pMSIG1.1-BRCA1-IRES-GFP retroviral construct was a generous gift of Dr. Ralph Scully. RAD51C cDNA was cloned in to the pMIG-IRES-GFP retroviral construct.

Plasmid transfections

Calcium phosphate-mediated transient transfection of ecotropic Bosc23 or amphotropic Phoenix packaging cells was performed as described before [2,11]. Retroviral particles were produced if necessary. Viral supernatants were harvested 36 hours later, filtered, and concentrated by centrifugation at 20,000 rpm for 2 hours at 14°C. Cells were infected twice a day for two days with a 1:1 mixture of concentrated virus and medium in the presence of 4μg/ml polybrene (Sigma). BCR-ABL1-positive UT7/9 cells were transfected with 5μg of pMIG1.1-IRES-GFP-BRCA1 DNA using Amaxa Human $CD34^+$ Cell Nucleofector Kit (Lonza). GFP^+, YFP+, and DsRed+ cells were isolated by flow cytometry and used for experiments.

Chemical inhibitors

RI-1 [16] was purchased from Sigma Chemicals and B02 was kindly obtained from Dr. Alexander Mazin [17]. Imatinib and ponatinib were purchased from LC Laboratories and all-trans retinoic-acid (ATRA) was from Sigma-Aldrich.

Table S1. Clinical annotation for the CML cases.

Diagnosis	ID	Molecular lesion	Karyotype
CML-CP	62	*BCR-ABL1*	46, XX, t(9;22)(q34;q11.2) / 45, X, -X
CML-CP	110	*BCR-ABL1*	46,XX,t(9,22)(q34;q11.2)
CML-CP	185	*BCR-ABL1*	46,XY,t(9;22)(q34;q11.2)
CML-CP	352	*BCR-ABL1*	46,XX,t(9;22)(q34;q11.2)
CML-CP	384	*BCR-ABL1*	46,XY, t(9;22)(q34;q11.2)
CML-CP	570	*BCR-ABL1*	Not available
CML-CP	586	*BCR-ABL1*	46,XX,t(9;22)(q34;q11.2)
CML-CP	589	*BCR-ABL1*	Not available
CML-CP	845	*BCR-ABL1*	46,XY, t(9;22)(q34;q11.2)
CML-CP	851	*BCR-ABL1*	Not available
CML-CP	852	*BCR-ABL1*	Not available
CML-CP	894	*BCR-ABL1*	46,XY, t(9;22)(q34;q11.2)
CML-CP	900	*BCR-ABL1*	Not available
CML-CP	925	*BCR-ABL1*	Not available
CML-CP	940	*BCR-ABL1*	Not available
CML-CP	954	*BCR-ABL1*	46,XY, t(9;22)(q34;q11.2)
CML-CP	107	*BCR-ABL1*	46,XY, t(9;22)
CML-CP	110	*BCR-ABL1*	46,XX, t(9;22)
CML-CP	111	*BCR-ABL1*	46,XX, t(9;22)
CML-CP	194	*BCR-ABL1*	46,XX, t(9;22)
CML-CP	264	*BCR-ABL1*	46,XY, t(9;22)
CML-CP	273	*BCR-ABL1*	46,XX, t(9;22)
CML-AP	701	*BCR-ABL1*	46,XX,inv(3)(q21q26),t(9;22)(q34;q11.2),i(17)(q10)
CML-AP	834	*BCR-ABL1*	Not available
CML-AP	101	*BCR-ABL1*	46,XX, t(9;22)
CML-AP	104	*BCR-ABL1*	46,XY t(9;22)
CML-AP	185	*BCR-ABL1*	46,XY, t(9;22)
CML-AP	239	*BCR-ABL1*	46,XY, t(9;22)

Table S2. Clinical annotation for the B-ALL cases studied in **Figure 5F, G** and **Figure S5**

Diagnosis	ID	Molecular lesion	Karyotype	Flow cytometry
B-ALL	ICN3	*MLL-AF4*	Not available	Not available
B-ALL	ICN12	*E2A-PBX1*	t(1;19)(q23;p13)	Not available
B-ALL	ICN13	*MLL-AF4*	t(4;11)(q21;q23)	Not available
B-ALL	LAX6	*IGH-TCRB*	t(7;14)(q34;q32)	Not available
B-ALL	LAX7	*Not available*	Not available	Not available
B-ALL	SFO1	*Not available*	Not available	Not available
B-ALL	LAX9	*BCR-ABL1*	t(9;22)(q34;q11)	Not available
B-ALL	PDX2	*BCR-ABL1*	Not available	CD10, CD19, CD22, CD34, cytoplasmic CD79a,dim CD123, HLA-DR, and TdT+
B-ALL	TXL3	*BCR-ABL1*	t(9;22)(q34;q11)	Not available
B-ALL	BLQ1	*BCR-ABL1 (T315I)*	der(9), der(22)	Not available
B-ALL	BLQ5	*BCR-ABL1 (T315I)*	der(9), der(22)	Not available
B-ALL	LAX2	*BCR-ABL1 (T315I)*	t(9;22)(q34;q11)	Not available

Table S3. Clinical annotation for the AML, B-ALL and T-ALL cases studied in **Figure 6**

Diagnosis	ID	NCI-Rome Risk Group/FAB	Molecular lesion	Karyotype	Flow cytometry
AML	9	M5	Unknown	Not available	CD11c, CD13, CD38, HLA-DR
AML	14	M2	Unknown	inv(3), -7	Not available
AML	201	Not available	Unknown	Del12(q13-q15)	CD13, CD33, CD34, CD117
T-ALL	4/10	Not available	Unknown	Normal	CD1a, CD2, CD3, CD4, CD5, CD7, CD8, CD10, CD33, CD34, CD38, CD45, CD71, CD99, CD117
T-ALL	15	Not available	Unknown	Not available	Not available
B-ALL	4	High	Unknown	inv(19)(p13.3q13.1)	CD10, CD19, CD20, CD22, CD34, CD45
B-ALL	16	High	Unknown	hyperdiploid 57-59 (+X, Y, 4, 6, 8, 9, 10, 14, 15, 17, 18, 21); t(1;19)	CD2, CD10, CD19, CD20, CD22, CD34, CD38, CD58, HLA-DR
B-ALL	17	High	Unknown	del(9p-)	CD10, CD11b, CD13, CD15, CD19, CD22, CD25, CD34, CD38, CD45, CD52, CD58, HLA-DR
B-ALL	21	High	p16 loss, IKAROS loss	del(9p)	CD9, CD10, CD11b, CD13, CD15, CD19, CD33, CD34, CD36, CD58, CD64, HLA-DR
B-ALL	23	Standard	Unknown	Normal	CD2, CD10, CD13, CD15, CD19, CD22, CD34, CD58, CD71, HLA-DR
B-ALL	43	Hgih	Unknown	11q23	NA
B-ALL	50	High	Unknown	Unknown	CD10, CD19, CD20, CD22, CD34, CD38, CD52

Table S4. Clinical annotation for the APL cases (>90% blasts).

Diagnosis	ID	Karyotype	Flow cytometry
APL	145	45,XY,t(15;17) (q22;q12), -19	CD13+, CD33+, CD34-, HLA-DR-
APL	1262	46,XX,t(15;17)(q22;q21)	CD10-, CD13+, CD14-, CD15 (dim) +, CD19-, CD20-, CD33+, CD34-, CD64-, CD79-, HLA-DR-, TdT-
APL	1113	46,XY,t(15;17)(q22;q21.1)	CD13 variable +, CD33+, CD34 subset ~8% +, CD64+, HLA-DR+

A

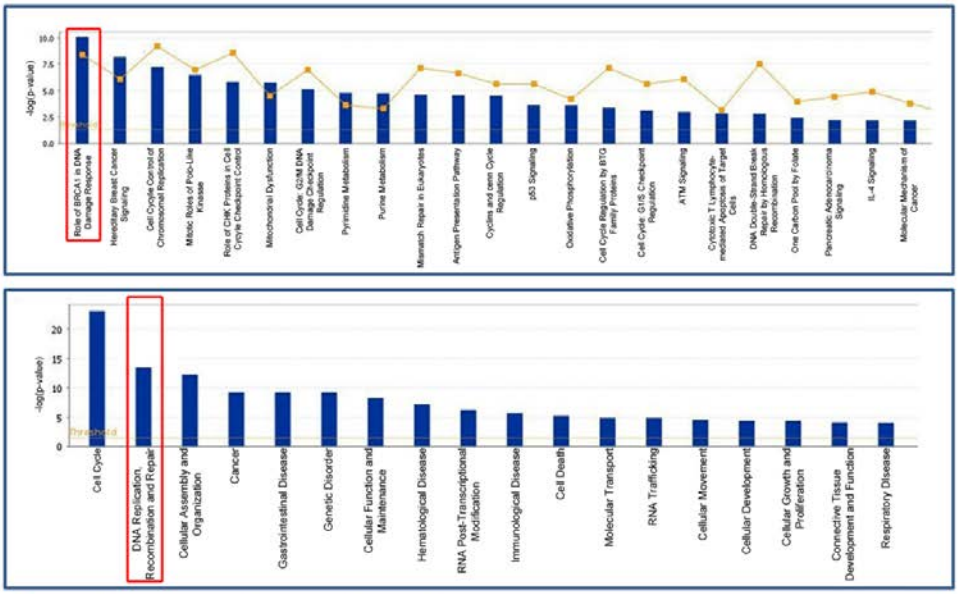

B

Gene	Pvalue	Fold change	Gene	Pvalue	Fold change	Gene	Pvalue	Fold change
RAD51	4.63E-09	7.62706	BLM	1.59E-05	2.86258	RPA1	0.0984566	1.52387
XRCC2	0.0002572	6.15298	LIG1	1.65E-05	2.79544	OBFC2B	0.0005633	1.51042
RAD51AP1	1.81E-07	5.62064	BRCA2	5.19E-06	2.7146	UBE2N	0.0049113	1.464
BRCA1	1.03E-06	5.39866	MMS22L	0.0002663	2.34486	PALB2	0.0207624	1.35896
RAD54B	1.09E-07	3.74303	H2AFX	0.0001790	1.94307	FAN1	0.0154917	1.3325
RAD54L	5.11E-06	3.58717	RPA2	0.0418216	1.55811			

C

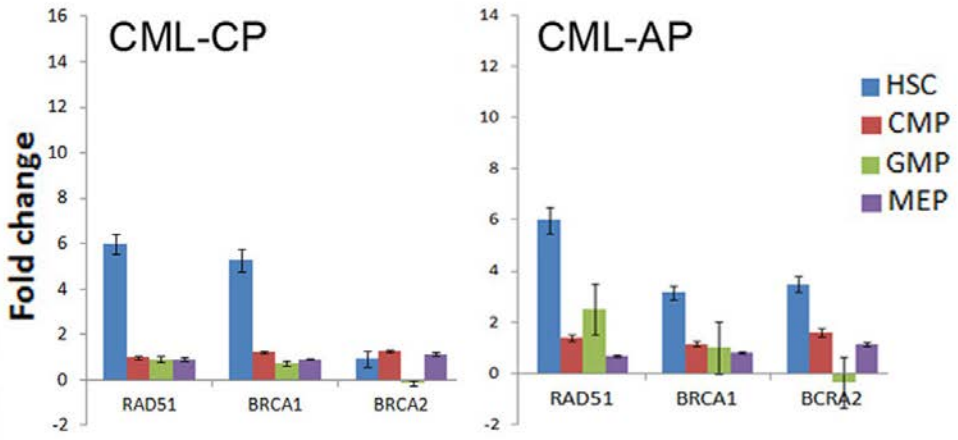

Figure S1. LSCs display elevated levels of expression of the genes involved in HRR. (**A**) Ingenuity pathway analysis of normal HSCs versus CML-CP LSCs: *Upper panel* - Canonical pathways, *Lower panel* - functional pathways; HRR pathways are highlighted in red boxes. (**B**) HRR genes found overexpressed in CML-CP LSCs compared with normal HSCs. (**C**) Validation of microarray expression data by qRT-PCR using the Fluidigm biomark platform. Relative expression of selected constituents of the HRR pathway was measured in stem and progenitor populations from patients with CML-CP and CML-AP and compared to cellular counterparts from healthy volunteers. Fold changes are expressed in terms of $2^{-\Delta\Delta Ct}$ relative to the calibrator population (equivalent healthy population). Each result is the mean +/- SEM of healthy, (n=3), CML-CP (n=6) and CML-AP (n=4) donor samples.

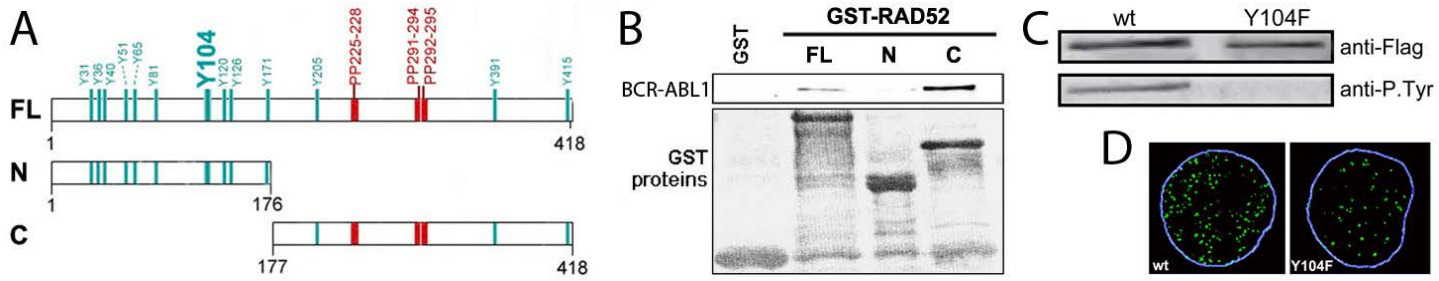

Figure S2. Moderate impact of BCR-ABL1 kinase interaction and phosphorylation of RAD52-Y104 on RAD52 foci formation. (**A**) GST-fusion proteins containing full-length RAD52 (FL) and the indicated fragments (N, C) were generated. The positions of tyrosine residues (Y) and proline-rich motif (PP) are indicated. (**B**) The fusion proteins were used for pull-down assay along with the total cell lysates from p210BCR-ABL1-32Dcl3 cells. The reactions were analyzed by Western blotting using anti-ABL antibody (BCR-ABL1 box); GST proteins were detected by Ponceau staining. (**C, D**) Flag-RAD52(wt) and Flag-RAD52(Y104F) mutant were expressed in BCR-ABL1-32Dcl3 cells. (**C**) Anti-Flag immunoprecipitates were analyzed by Western blotting to detect Flag-RAD52 (upper box) and tyrosine phosphorylated RAD52 (lower box). (**D**) Flag-RAD52(wt) and Flag-RAD52(Y104F) foci were detected by anti-Flag immunofluorescence in BCR-ABL1-32Dcl3 cells 4 hours after irradiation with 4Gy. Representative nuclei are presented.

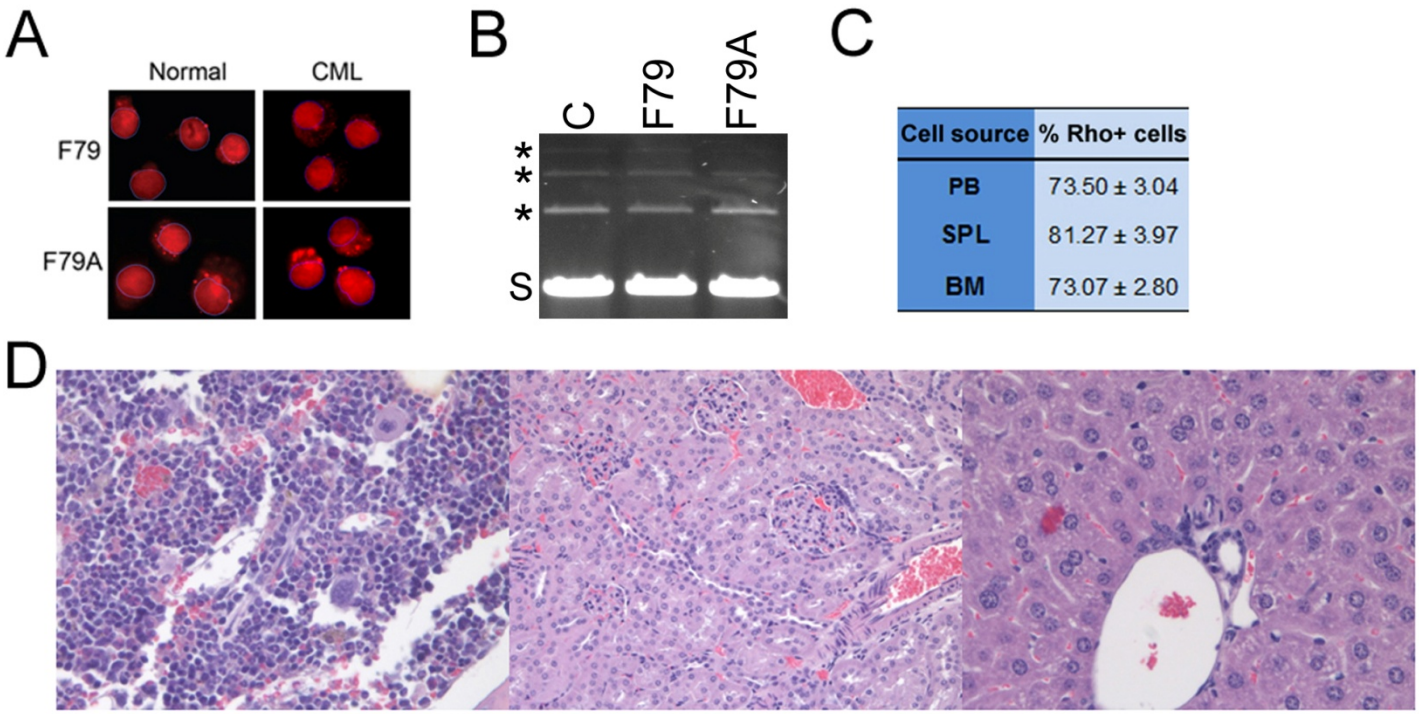

Figure S3. Efficient cellular uptake and lack of toxicity of aptamer F79 to normal tissues. (**A**) $Lin^{-}CD34^{+}$ cells from bone marrow of normal donor and CML-CP patient were incubated with 5 μM of either the F79 or F79A rhodamine (Rho)-conjugated aptamer for 1 hr. DNA was counterstained with DAPI. Aptamer uptake was visualized by fluorescence; nuclei borders are marked in blue. (**B**) F79 does not affect NHEJ; S=substrate, products are marked by asterisks. (**C**) Three SCID mice were injected intravenously with 2.5 mg/kg F79 aptamer daily for 3 days. Mice were sacrificed 24 hrs after last injection and the percentage of rhodamine (Rho)-positive cells (± SD) in peripheral blood (PB), spleen (SP), and bone marrow (BM) was determined by flow cytometry. (**D**) H&E sections (40x) of (*left panel*) bone marrow showing trilineage hematopoiesis, (*middle panel*) kidney and (*right panel*) liver from F79-treated mice with no specific pathologic changes.

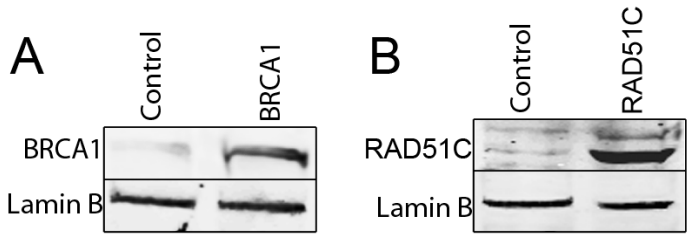

Figure S4. Restoration of BRCA1 and RAD51C protein expression levels. (**A**) BCR-ABL1 –positive UT7/9 cells and (**B**) PML-RAR –positive NB4 cells were transfected with retroviral construct encoding GFP (Control) and BRCA1-IRES-GFP (BRCA1) or RAD51C-IRES-GFP (RAD51C), respectively. Nuclear extracts were analyzed by Western blotting to detect BRCA1, RAD51C, and lamin B (loading control).

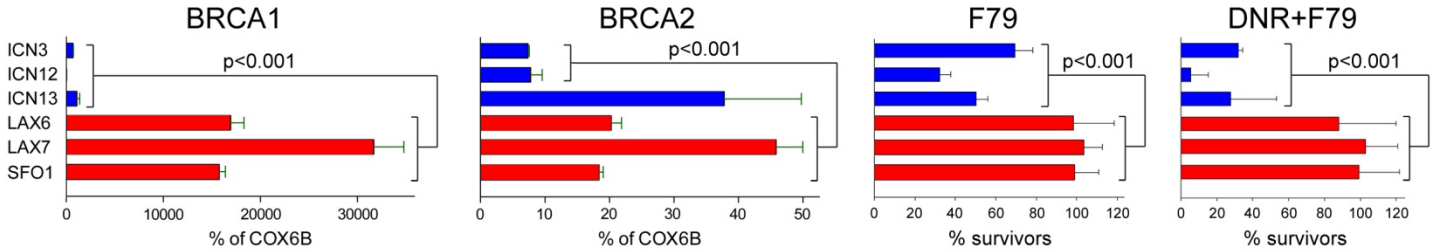

Figure S5. BRCA1 mRNA levels pre-determine the sensitivity of BCR-ABL1 -negative B-ALL xenograft cells to F79 aptamer. (*BRCA1 and BRCA2 panels*) BRCA1 and BRCA2 mRNA were detected by qRT-PCR in 6 Philadelphia chromosome-negative B-ALL xenografts harvested from NSG mice. Results represent mean expression levels ± SD. (*F79 and DNR+F79 panels*) BRCA1 and/or BRCA2 "low" (blue), and BRCA1 and BCRA2 "high" (red) xenograft cells were incubated with 5μM of F79 aptamer (*F79 panel*) or 0.1μM daunorubicin + 5μM F79 aptamer (*DNR+F79 panel*). Results represent mean percentage of surviving cells ± SD from triplicate experiments per patient when compared to untreated (*F79 panel*) and DNR-treated (*DNR+F79*) samples.

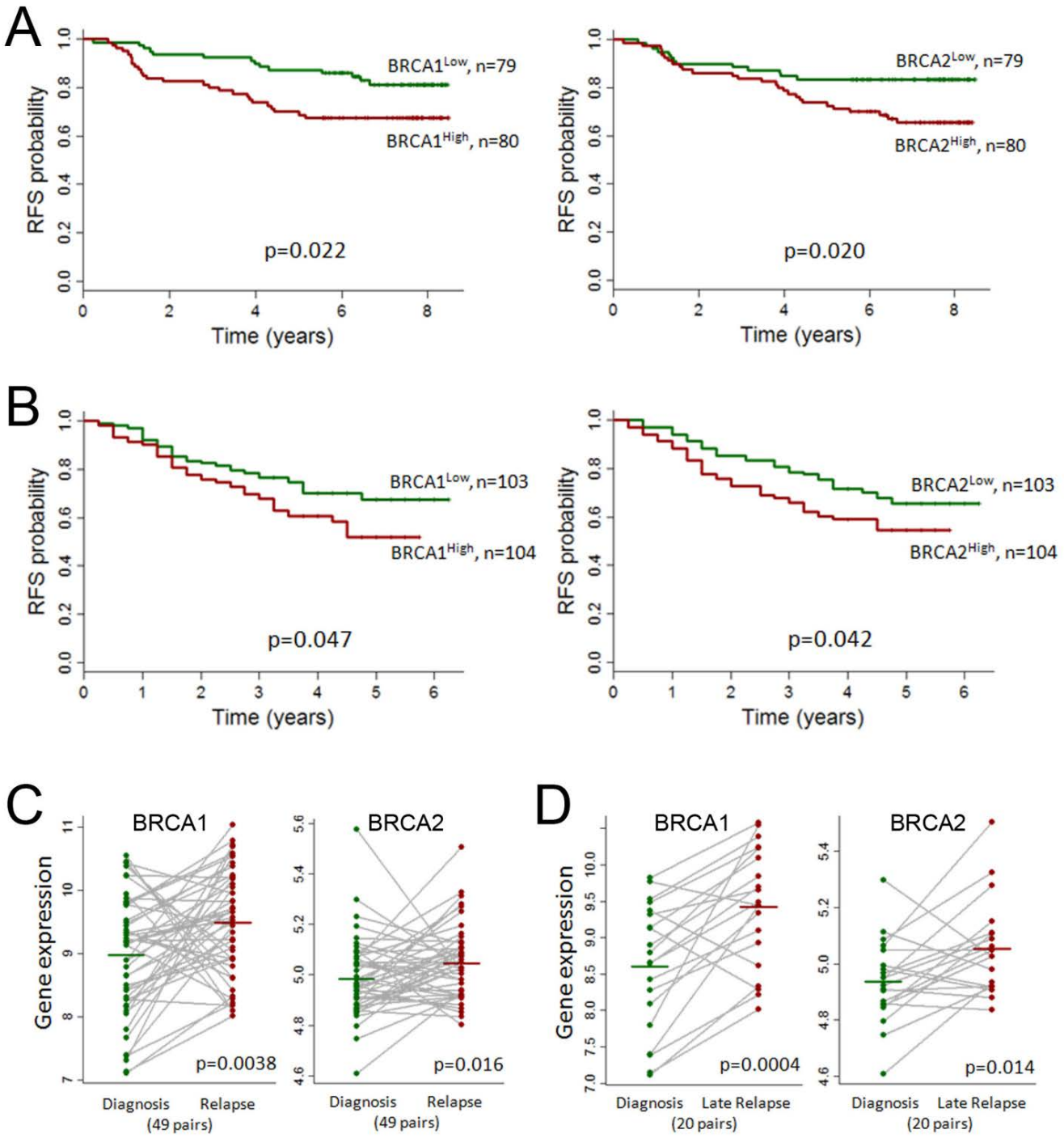

Figure S6. Prognostic value of the expression levels of BRCA1 and BRCA2. (**A**, **B**) Kaplan-Meier estimates of relapse free survival (RFS) for patients with (**A**) breast carcinoma and (**B**) pediatric B-precursor ALL, based on BRCA1 or BRCA2 mRNA expression levels. The patients were divided into two groups based on higher or lower than the median gene expression values for BRCA1 or BRCA2; p values were calculated from the logrank test. (**C**, **D**) Expression of BRCA1 and BRCA2 mRNA in matched diagnosis-relapse pediatric B-precursor ALL: (**C**) diagnosis –relapse (including both early (<36 months) and late relapse (>36 months)), and (**D**) diagnosis – late relapse (>36 months); p values were calculated from two-sided Wilcoxon test. Analyses were performed using previously published arrays: (A) [18], (B) [19], and (C, D) [20].

Video 1. Computer modeling of the interaction of aptamer F79 with RAD52 protomers. We extracted three chains (A, B and K) from the undecameric crystal structure of the N-terminal annealing domain of human RAD52 and then cut away the middle chain A to reveal the location of the 13 residues in chain B corresponding to the F79 aptamer (Figure 3B). The 13 residues make up part of the monomer-monomer binding interface [21,22]. Modeling of the F79 aptamer suggests that it can mimic these 13 residues and bind to the neighboring subunit, thereby blocking the binding of one monomer to the other. The size of the buried surface area of the F79 aptamer (530 Å^2) appears adequate to affect disruption of the protein-protein interaction represented by monomer-monomer binding (buried surface area = approximately 2,600 Å^2). In addition, a number of favorable binding interactions between the F79 aptamer and the RAD52 subunit were identified by interface analysis, including a key interaction between the aptamer tyrosine corresponding to Y81 and the natural Y81 binding pocket on the neighboring subunit [23]. In this model, the aptamer phenylalanine residue corresponding to F79 protrudes out into the binding domain and cannot be accommodated by the opposing subunit face. This bulky benzyl group may play a significant role in prohibiting subunit binding, thus reducing ssDNA binding by preventing or destabilizing the oligomeric assembly of RAD52.

Supplemental References

1. Stark JM, Pierce AJ, Oh J, Pastink A, Jasin M. Genetic steps of mammalian homologous repair with distinct mutagenic consequences. *Mol Cell Biol*. 2004;24(21):9305-9316.
2. Nieborowska-Skorska M, Kopinski PK, Ray R, et al. Rac2-MRC-cIII-generated ROS cause genomic instability in chronic myeloid leukemia stem cells and primitive progenitors. *Blood*. 2012;119(18):4253-4263.
3. Koptyra M, Falinski R, Nowicki MO, et al. BCR/ABL kinase induces self-mutagenesis via reactive oxygen species to encode imatinib resistance. *Blood*. 2006;108(1):319-327.
4. Nowicki MO, Falinski R, Koptyra M, et al. BCR/ABL oncogenic kinase promotes unfaithful repair of the reactive oxygen species-dependent DNA double-strand breaks. *Blood*. 2004;104(12):3746-3753.
5. Skorski T, Kanakaraj P, Nieborowska-Skorska M, et al. p120 GAP requirement in normal and malignant human hematopoiesis. *J Exp Med*. 1993;178(6):1923-1933.
6. Deutsch E, Jarrousse S, Buet D, et al. Down-regulation of BRCA1 in BCR-ABL-expressing hematopoietic cells. *Blood*. 2003;101(11):4583-4588.
7. Feng Z, Scott SP, Bussen W, et al. Rad52 inactivation is synthetically lethal with BRCA2 deficiency. *Proc Natl Acad Sci U S A*. 2011;108(2):686-691.
8. DelloRusso C, Welcsh PL, Wang W, Garcia RL, King MC, Swisher EM. Functional characterization of a novel BRCA1-null ovarian cancer cell line in response to ionizing radiation. *Mol Cancer Res*. 2007;5(1):35-45.
9. Scully R, Ganesan S, Vlasakova K, Chen J, Socolovsky M, Livingston DM. Genetic analysis of BRCA1 function in a defined tumor cell line. *Mol Cell*. 1999;4(6):1093-1099.
10. Flis K, Irvine D, Copland M, Bhatia R, Skorski T. Chronic myeloid leukemia stem cells display alterations in expression of genes involved in oxidative phosphorylation. *Leuk Lymphoma*. 2012;53(12):2474-2478.
11. Slupianek A, Dasgupta Y, Ren SY, et al. Targeting RAD51 phosphotyrosine-315 to prevent unfaithful recombination repair in BCR-ABL1 leukemia. *Blood*. 2011;118(4):1062-1068.
12. Slupianek A, Schmutte C, Tombline G, et al. BCR/ABL regulates mammalian RecA homologs, resulting in drug resistance. *Mol Cell*. 2001;8(4):795-806.
13. Wang Q, Zhang H, Guerrette S, et al. Adenosine nucleotide modulates the physical interaction between hMSH2 and BRCA1. *Oncogene*. 2001;20(34):4640-4649.
14. Slupianek A, Nowicki MO, Koptyra M, Skorski T. BCR/ABL modifies the kinetics and fidelity of DNA double-strand breaks repair in hematopoietic cells. *DNA Repair (Amst)*. 2006;5(2):243-250. Epub 2005 Nov 2016.
15. Grimme JM, Honda M, Wright R, et al. Human Rad52 binds and wraps single-stranded DNA and mediates annealing via two hRad52-ssDNA complexes. *Nucleic Acids Res*. 2010;38(9):2917-2930.
16. Budke B, Logan HL, Kalin JH, et al. RI-1: a chemical inhibitor of RAD51 that disrupts homologous recombination in human cells. *Nucleic Acids Res*. 2012.
17. Huang F, Mazina OM, Zentner IJ, Cocklin S, Mazin AV. Inhibition of homologous recombination in human cells by targeting RAD51 recombinase. *J Med Chem*. 2012;55(7):3011-3020.
18. Pawitan Y, Bjohle J, Amler L, et al. Gene expression profiling spares early breast cancer patients from adjuvant therapy: derived and validated in two population-based cohorts. *Breast Cancer Res*. 2005;7(6):R953-964.
19. Kang H, Chen IM, Wilson CS, et al. Gene expression classifiers for relapse-free survival and minimal residual disease improve risk classification and outcome prediction in pediatric B-precursor acute lymphoblastic leukemia. *Blood*. 2010;115(7):1394-1405.
20. Hogan LE, Meyer JA, Yang J, et al. Integrated genomic analysis of relapsed childhood acute lymphoblastic leukemia reveals therapeutic strategies. *Blood*. 2011;118(19):5218-5226.
21. Kagawa W, Kurumizaka H, Ishitani R, et al. Crystal structure of the homologous-pairing domain from the human Rad52 recombinase in the undecameric form. *Mol Cell*. 2002;10(2):359-371.
22. Singleton MR, Wentzell LM, Liu Y, West SC, Wigley DB. Structure of the single-strand annealing domain of human RAD52 protein. *Proc Natl Acad Sci U S A*. 2002;99(21):13492-13497.
23. Lloyd JA, McGrew DA, Knight KL. Identification of residues important for DNA binding in the full-length human Rad52 protein. *J Mol Biol*. 2005;345(2):239-249.